Highlights of the 28th annual meeting of the American Society of Neuroradiology. Los Angeles, March 19-23, 1990. Proceedings.

AJNR Am J Neuroradiol 1990, 11 (5) 1057-1068
http://www.ajnr.org/content/11/5/1057.citation

ASNR Section

Highlights of the 28th Annual Meeting of the American Society of Neuroradiology, Los Angeles, March 19–23, 1990

Michael S. Huckman,[1] Jamshid Ahmadi,[2] Mary Kay Edwards,[3] Olof Flodmark,[4] Glenn S. Forbes,[5] Allen J. Fox,[6] Carlos F. Gonzalez,[7] David B. Hinshaw,[8] Walter Kucharczyk,[9] Richard E. Latchaw,[10] Benjamin C. P. Lee,[11] M. Judith Donovan Post,[12] and Charles M. Strother[13]

After a superb categorical course on brain tumors (see page 1069), the scientific sessions began on Monday morning, March 19, 1990. In addition to 151 scientific papers, the program included four posters, 36 excerpta extraordinaire, 73 scientific exhibits, 40 technical exhibits, four special focus lectures, the President's Lecture, and presentation of the Cornelius G. Dyke Award paper. Although most lectures and reports were presented during plenary sessions, Thursday afternoon sessions on head and neck radiology, MR angiography, interventional neuroradiology, and excerpta extraordinaire were presented concurrently.

This report is a summary of some of the papers and lectures the program committee considered particularly noteworthy because of their originality or broad scope of interest or because the material for any number of reasons merited broad exposure.

MR Imaging of the Motion of Body Fluids

A number of sessions were devoted to MR imaging of the motion of body fluids, which included arterial and venous blood flow, CSF movement, and molecular diffusion. The opening three sessions were devoted to technical papers on MR angiography and included time-of-flight and phase-contrast depiction of vessels, two- and three-dimensional Fourier transform (2DFT and 3DFT) data acquisitions, and plain and gadopentetate dimeglumine contrast-enhanced imaging. Tsuruda et al. (San Francisco) presented a method by which multiple sections of a three-dimensional (3D) time-of-flight MR angiogram and a maximum intensity ray-tracing algorithm were combined to produce conventional angiogramlike images (Fig. 1). Despite the excellent quality of these images, artifacts due to the loss of low-intensity features caused

[1] Rush-Presbyterian-St. Lukes's Medical Center, 1653 W. Congress Parkway, Chicago, IL 60612.
[2] University of Southern California, School of Medicine, Los Angeles, CA 90039.
[3] Indiana University School of Medicine, Indianapolis, IN 46202.
[4] Karolinska Hospital, Stockholm, S-104 01 Sweden.
[5] Mayo Clinic, Rochester, MN 55901.
[6] University Hospital, London, Ontario N6A 5A5, Canada.
[7] Thomas Jefferson University Hospital, Philadelphia, PA 19107.
[8] Loma Linda University Medical Center, Loma Linda, CA 92354.
[9] Toronto General Hospital, Toronto, Ontario M5G 2C4, Canada.
[10] Englewood, CO 80111.
[11] University of Minnesota Hospital, Minneapolis, MN 55455.
[12] University of Miami, Miami, FL 33101.
[13] University of Wisconsin, Madison, WI 53792.

AJNR 11:1057–1068, September/October 1990 0195–6108/90/1105–1057

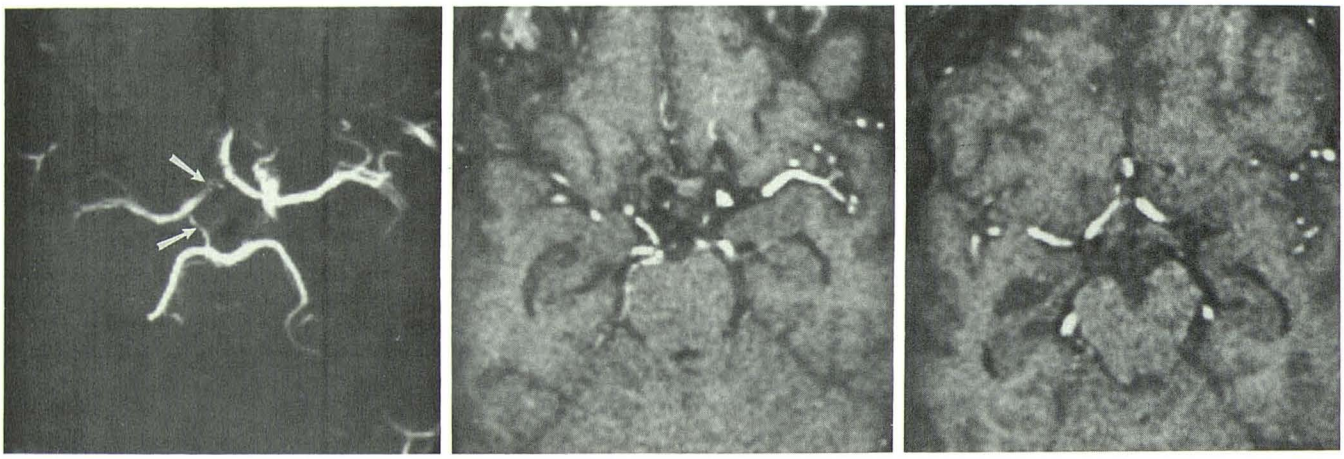

Fig. 1.—Maximum intensity projection (MIP) artifact in MR angiograms.
***A*, MIP projection of circle of Willis in a patient with occlusion of right internal carotid artery shows narrowing of right A1 segment and questionably decreased flow in right posterior communicating artery (*arrows*). Projection was constructed from 60 individual partitions by using a three-dimensional time-of-flight acquisition.**
***B* and *C*, Individual partitions through both areas shown in *A* give a truer rendition of these vessels.**

overestimation of stenoses and suboptimal visualization of small vessels and intraluminal detail. Edelman et al. (Boston) found that their method of "black blood" MR angiography avoided problems arising from the signal loss due to turbulence encountered in "bright blood" angiography. The black blood technique was particularly good for demonstration of severely stenotic vessels.

A number of papers indicated strong attempts to bring MR angiography above the research threshold and into the clinical mainstream. Mawad and Nitz (Houston) reviewed 100 intracranial 3D MR angiographic studies and reported high sensitivity for the detection of small aneurysms and adequate evaluation of the relationship of sellar and parasellar neoplasms to the carotid arteries.

Fram et al. (Phoenix) and Chao et al. (Philadelphia) showed consistent visualization of intracranial aneurysms. Litt et al. (New York) demonstrated good correlation between 3DFT MR angiography and contrast angiography in the detection and definition of clinically significant carotid arterial stenosis. Hinshaw et al. (Loma Linda) found that 3DFT MR angiography was highly useful in the preoperative evaluation of head and neck neoplasms, and in most cases it obviated conventional angiography (Fig. 2).

Current applicability of MR angiography resembles a "moving target." Techniques are evolving rapidly, and minor changes in sequence details can make an enormous difference in image quality. At this time, no standardization of technique exists among centers and manufacturers who are engaged in evaluating this imaging technique.

CSF flow dynamics were studied by Bradley et al. (Long Beach). Using T2-weighted spin-echo MR images, they examined the hyperdynamic CSF flow state by identifying the aqueduct flow void sign in patients who had had shunts placed because of normal-pressure hydrocephalus. Patients with marked flow void tended to do well after placement of a shunt, whereas those with a normal flow void were unlikely to have a good outcome. These results indicate that the predictive value of MR imaging in normal-pressure hydrocephalus may match or exceed that of CT and radioisotopic cisternography.

Kucharczyk et al. (San Francisco) evaluated an experimental canine stroke model with diffusion-weighted MR imaging and found that lesions produced by occlusion of the middle cerebral artery consistently were observed much earlier on diffusion-weighted images than they were on T2-weighted images (Fig. 3). They then used this model to show how cerebral injury could be ameliorated by treating ischemic lesions with calcium channel blockers.

Anatomy, Embryology, and Pediatric Neuroradiology

Truwit and Barkovich (San Francisco) gave an outstanding presentation on the subject of intracranial lipomas (see *AJNR* July/August 1990). Hypothesizing that lipomatous tissue found intracranially represents congenital malformations, the authors were able to show that the most common locations for these lesions correlated with the areas in which the dissolving meninx primitiva remains the longest (i.e., in the interhemispheric fissure). They concluded that intracranial lipomas are true congenital malformations that form in the subarachnoid space, not mesodermal elements that are included during closure of the neural tube. These lipomas typically are traversed by nerves and vessels (Fig. 4).

The same authors studied 23 infants, of various gestational ages at birth, who had suffered hypoxic or ischemic injury to the brain during the perinatal period. The patterns of abnormalities were related not only to the likely degree and mechanism of the injury but also to the degree of maturity of the brain at the time of birth (i.e., lesions of different morphology were seen in premature infants compared with the patterns seen in term infants). MR imaging performed during childhood

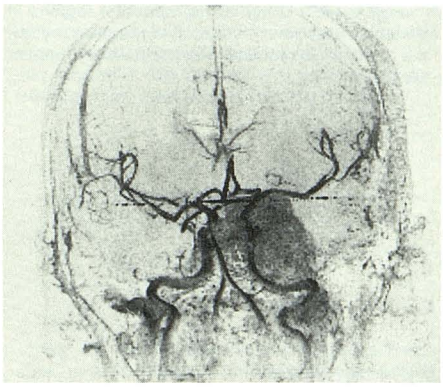

Fig. 2.—Coronal, fast low-angle shot, three-dimensional Fourier transform MR angiogram shows displacement of basilar artery and attenuation of flow in left cavernous carotid artery by a large petrous apex osteochondroma. Tumor blush is produced by simultaneous use of gadopentetate dimeglumine.

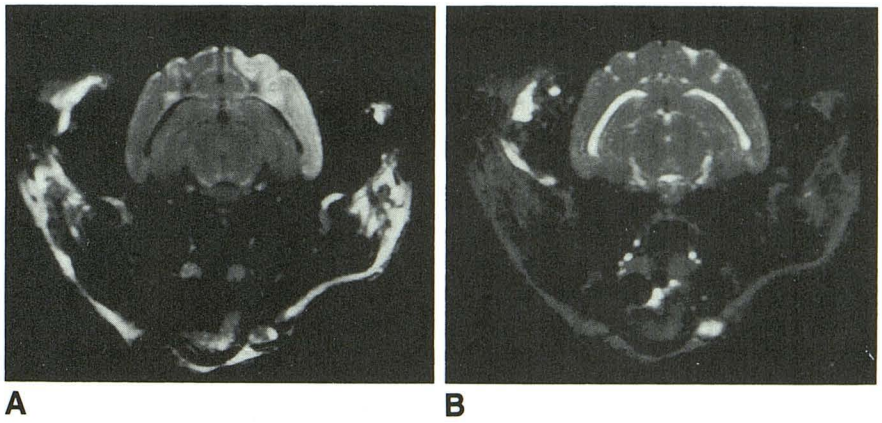

A B

Fig. 3.—Diffusion-weighted MR imaging, which is sensitive to changes in microscopic motion of water protons rather than increased water content per se, can detect cerebral ischemia well in advance of T2-weighted spin-echo MR imaging.

A, Coronal diffusion-weighted MR image, 1800/80, of cat brain obtained 45 min after unilateral occlusion of middle cerebral artery shows clearly visible intense signal throughout cortical territory of occluded artery.

B, T2-weighted MR image, 2800/160, taken 20 min after *A* shows no signal.

Fig. 4.—Coronal spin-echo MR image, 600/20, shows lipoma of left internal auditory meatus. Note seventh and eighth cranial nerve complex traversing lipoma rather than being displaced by it (*arrow*). This is typical of intracranial lipomas and is consistent with concept of abnormal development of subarachnoid cisterns, whereby meninx primitiva fails to completely resorb and maldifferentiates into a lipoma.

Fig. 5.—T2-weighted MR image at level of centrum semiovale shows periventricular high signal, which is part of pattern of brain damage caused by perinatal hypoxic or ischemic injury in an infant born prematurely.

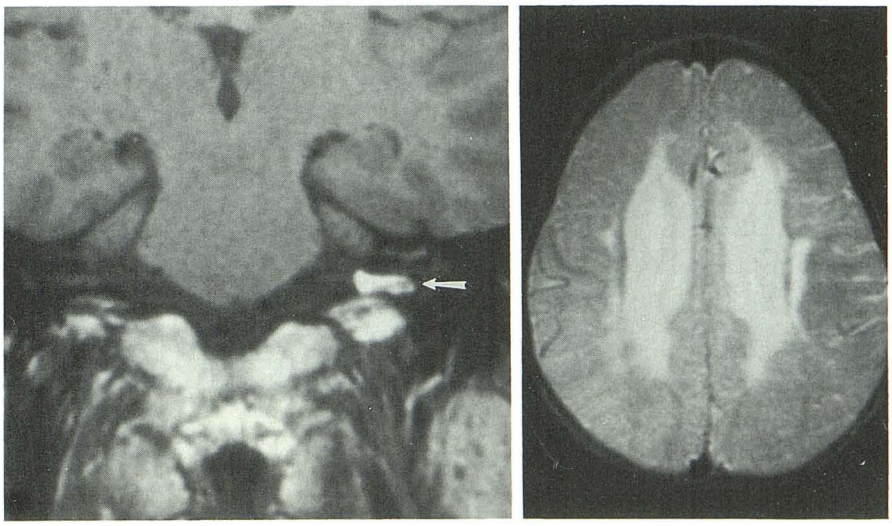

4 5

gave an indication about how and when the brain injury occurred. Although this evaluation gives information about the stage of brain maturation at the time of injury, it provides no information about the circumstances under which the injury occurred (Figs. 5 and 6). Edwards et al. (Indianapolis) presented four patients with cerebral cortical laminar necrosis. MR scans showed cortical and subcortical T1 and T2 shortening due to hemorrhage. This appearance, which generally is caused by an anoxic event, is seen also in association with "shaken baby" syndrome. The damage is thought to be due to chest or neck compression with resultant hypoxia rather than direct intracranial brain battering (Fig. 7).

The 1990 Cornelius G. Dyke Award was given to M. D. Nelson, Jr., of Children's Hospital of Los Angeles for his paper titled "The Search for Human Telencephalic Ventriculofugal Arteries." Brains from fetuses and children of various ages were studied by using microfil injection, thick sections of the brain, and immunohistologic and histochemical identification of developing blood vessel walls. Using these methods, Nelson and his coworkers were unable to identify any vessels that originated in the choroid plexus, crossed the ventricle, and penetrated the ependyma from the ventricular side. They concluded that their study could not support the concept of ventriculofugal arteries in the human fetus and infant.

Degenerative Disorders

Several papers on degenerative disorders and associated white matter conditions were of particular interest. Kikinis et al. (Boston) reported small differences in MR measurements of ventricular and extracerebral CSF space among groups of

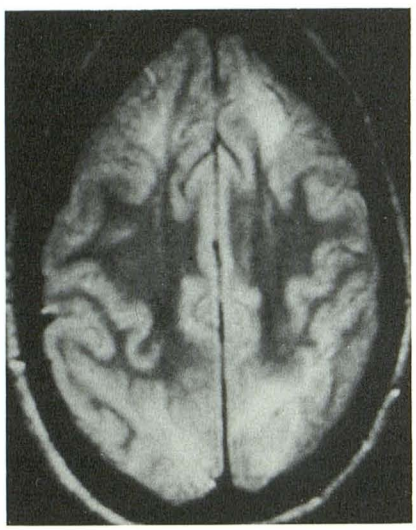

6

7

Fig. 6.—MR image of high parietal regions in an infant born near term shows prominent cortical damage associated with perinatal hypoxic or ischemic injury.

Fig. 7.—MR image of 2-month-old victim of child abuse shows hemorrhage in gray matter in a multifocal distribution with increased signal due to deoxyhemoglobin.

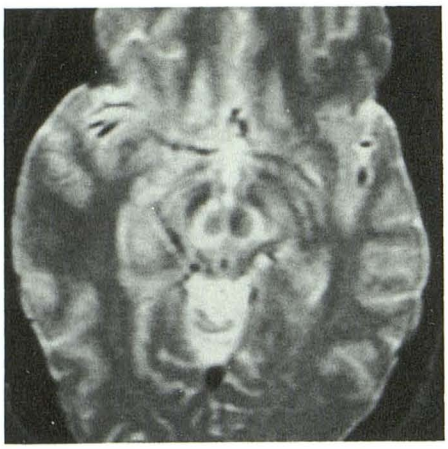

A

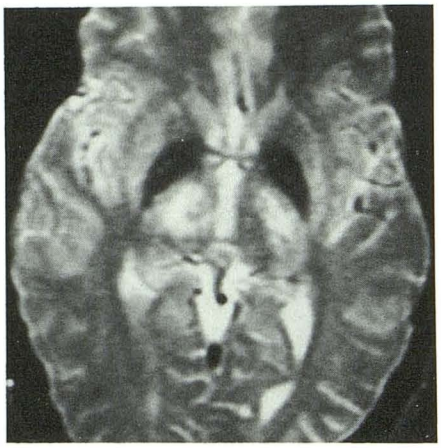

B

Fig. 8.—*A* and *B*, T2-weighted MR images, 3000/90, in a 24-year-old with Wilson disease show increased signal intensity in mesencephalon surrounding red nuclei and low signal intensity in the substantia nigra (*A*); decreased signal intensity in globus pallidus; and increased signal intensity in putamen, posterior limb of internal capsule, and thalamic nuclei (*B*).

patients who had normal-pressure hydrocephalus, Alzheimer disease, or brain atrophy. In the discussion after the presentation, the authors agreed that specific measurements are not yet useful in the selection of individual patients for shunting. The body of information on direct histopathologic correlation of white matter changes in Alzheimer disease was enhanced further by the study of Bowen et al. (Miami). Foci of T2-weighted hyperintensity were increased in patients with hypertension or Alzheimer disease when the findings were compared with the results of antemortem or postmortem studies of elderly control patients. Vascular risk factors continue to be associated with the greatest number of white matter changes.

Medial temporal lobe volumes were assessed by Ashtari et al. (New Hyde Park, NY), who suggested that the volumes of the hippocampus and amygdala are smaller than normal in patients with Alzheimer disease. The discussion after their presentation questioned the exclusion of parts of the anatomic hippocampus in their technique.

A special focus lecture delivered by Davies (New York) showed the neuritic plaques and neurofibrillary tangles present throughout the course of Alzheimer disease and emphasized that typical amyloid deposition in cerebral vessels is common both in patients who have this disease and in elderly persons who do not. He stated that future diagnostic tests will need to be directed toward the detection of specific protein abnormalities in the brains of patients who have dementia. As many amyloid precursors and tangled protein components are common throughout the body, recent developments in monoclonal antibody technology suggest that these precursors and components may be helpful for detection and imaging in the brain.

A paper by Brunberg et al. (Ann Arbor) presented excellent images showing decreased T2 signal changes in the basal ganglia in Wilson disease that were seen at 1.5 T but not at 0.35 T (Fig. 8). Small foci of increased T2 signal representing small degenerative cysts in the outer putamen, midbrain, and pons were shown also. Diffuse atrophic changes with hyper-

Fig. 9.—MR image, 2000/50, in a patient with olivopontocerebellar atrophy shows increased signal intensity in transverse pontine fibers, middle cerebellar peduncles, and cerebellum. Pyramidal tracts and tegmentum are normal.

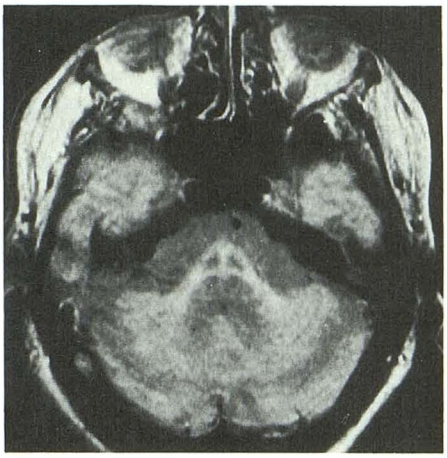

9

Fig. 10.—MR image shows enlarged perivascular spaces (*arrows*) surrounding penetrating branches of collicular arteries, which account for punctate and linear foci of abnormal signal in midbrains of about 20% of control subjects.

10

Fig. 11.—Axial postcontrast T1-weighted MR image shows enhancing venous plexus (*arrows*) surrounding nonenhancing hypoglossal nerves in a tubular configuration. An acoustic schwannoma compresses left cisternal segment of hypoglossal nerve.

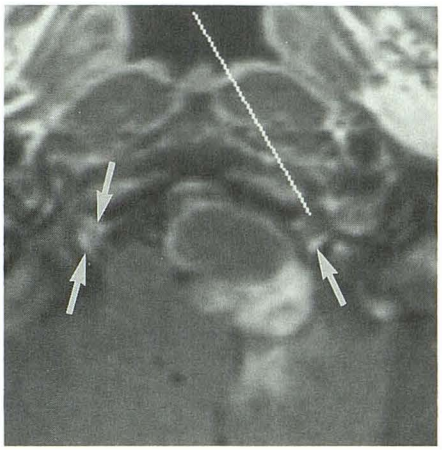

11

Fig. 12.—Coronal postcontrast T1-weighted image shows enhancing venous plexus (*arrowheads*) surrounding filling defect of right hypoglossal nerve, creating a "target sign." An acoustic schwannoma compresses cisternal segment of left hypoglossal nerve. Note cranial nerves IX, X, and XI (*open arrow*) exiting jugular foramen and joining cranial nerve XII (*solid arrow*) within left carotid sheath.

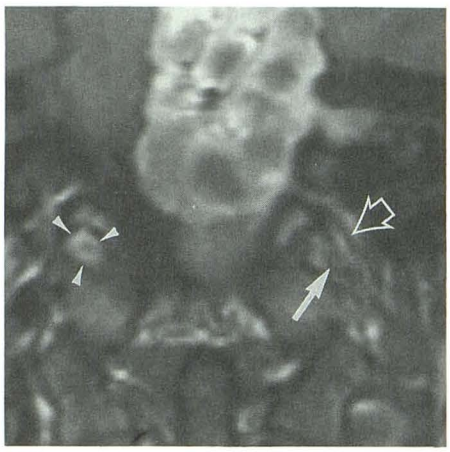

12

intense T2 foci in the brainstem were seen by Savoiardo et al. (Milan) in multisystem atrophy (Fig. 9), and a potentially new perspective on the role of corpus callosum impingement in producing axonopathy from hydrocephalus was presented by Jinkins (San Antonio). An interesting set of observations on hyperintense T2 foci in the midbrain (Fig. 10) was provided by Elster and Richardson (Winston-Salem). This report correlated changes on MR images with detailed anatomic studies from other cadaveric specimens to link such midbrain foci with enlarged perivascular spaces in many normal cases.

Otorhinolaryngologic Radiology

The two sessions devoted to otorhinolaryngologic radiology began with a preliminary report by Abrahams et al. (New Haven) on the efficacy of off-line processing of CT data for full mandibular display in the assessment of neoplasms. Excellent examples of CT reconstructions of complex orbital facial fractures were presented by Schellhas et al. (St. Louis Park, MN), indicating the potential sequelae of ostiomeatal obstruction and recurrent sinus infection.

Point et al. (Baltimore) presented a report on the insensitivity of MR imaging for the routine evaluation of dysphagia. However, they did show that MR could be used to characterize abnormalities when a lesion was present. Dalley et al. (Seattle) presented an excellent anatomic study of normal and pathologic conditions of the hypoglossal canal, emphasizing the role of gadopentetate dimeglumine enhancement in outlining the hypoglossal venous plexus (Figs. 11 and 12). Smoker et al. (Salt Lake City) showed that numerous lesions are responsible for hypoglossal neuropathy (Fig. 13). Both their paper and work by Tryhus et al. (Salt Lake City), which evaluated Horner syndrome, underscored the complex anatomy and clinical presentations of disorders of the lower cranial nerves.

Excellent thin-section high-resolution MR images of the petrous bone and otic capsule structures were presented by Brogan et al. (Columbus). Images were obtained by using a 3DFT gradient-echo technique (33/7/1, 15° flip angle, and a slice thickness of 0.5–1.0 mm). The resolution of these thin-section images approached or surpassed that of CT scans (Fig. 14). The facial nerve, cochlea, and the vestibular and cochlear aqueducts were visualized, providing the potential

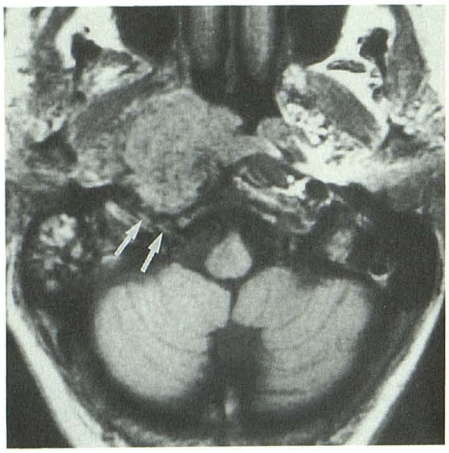

13

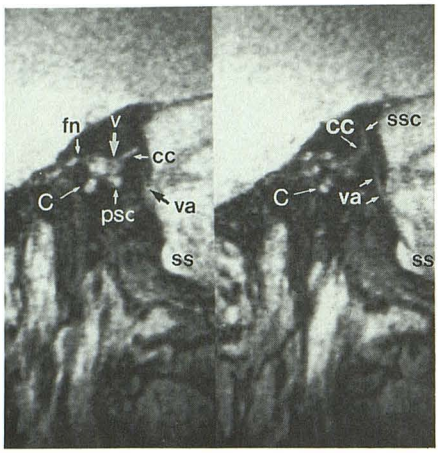

14

Fig. 13.—T1-weighted MR image of 74-year-old man who had isolated right hypoglossal neuropathy shows a large mass that fills nasopharyngeal carotid space and extends posteriorly to about right hypoglossal nerve as it traverses hypoglossal canal (*arrows*). Diagnosis was nasopharyngeal squamous cell carcinoma.

Fig. 14.—Normal temporal bone. Sagittal, three-dimensional Fourier transform, gradient-echo MR images, 33/7/1, 15° flip angle, 1.0-mm slice thickness, at level of vestibule (v) and vestibular aqueduct (va). Endolymphatic duct and sac appear as high signal within vestibular aqueduct, which is seen coursing posteriorly and inferiorly from region of common crus (cc) to open into posterior cranial fossa near sigmoid sinus (ss). Common crus and superior semicircular canal (ssc) arise from vestibule. Labyrinthine portion of facial nerve (fn), posterior semicircular canal (psc), and cochlea (c) are seen also.

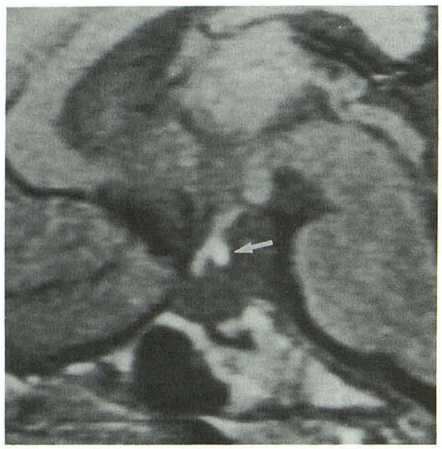

A

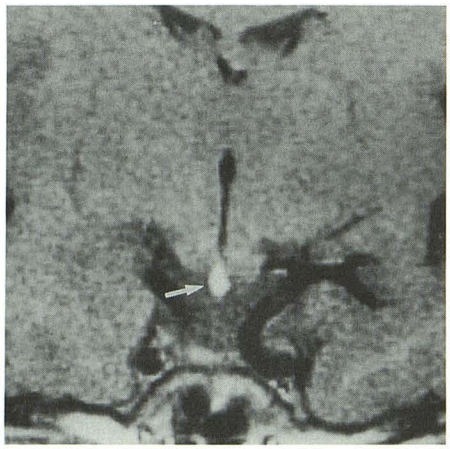

B

Fig. 15.—Ectopic neurohypophysis.

A, Sagittal T1-weighted MR image shows abnormal bright signal near median eminence (*arrow*). Note absence of infundibular stalk and small anterior pituitary gland.

B, Coronal T1-weighted MR image confirms abnormal bright signal of ectopic neurohypophysis (*arrow*) with no infundibulum and a thin anterior pituitary gland.

for assessing abnormalities of these structures directly rather than observing their secondary effects on surrounding bone.

A special focus lecture on the imaging of cervical lymph nodes was delivered by Som (New York). He spent considerable time stressing the importance of the anatomic location and organization of cervical lymph nodes. He related the importance of this for pretreatment cancer staging.

Sella Turcica

An abnormality of the hypothalamus associated with growth hormone deficiency was described by Abrahams et al. (Columbus). An ectopic neurohypophysis, defined as T1 bright signal near the median eminence, absent infundibulum, and absent posterior pituitary bright signal, was found in 39% of patients with idiopathic growth hormone deficiency (Fig. 15). Nine patients in the series had multiple hormone deficiencies, and all nine had an ectopic neurohypophysis.

The latest chapter in the saga of the bright signal of the neurohypophysis was delivered in a paper by Kucharczyk et al. (Toronto). The controversy about the source of the bright signal in the posterior pituitary was addressed once again, and a lipid, rather than protein or vasopressin, was proposed as the source of the signal. MR images were obtained of various concentrations of phospholipid vesicles similar to those present in the neurohypophysis. The characteristics of the phospholipid vesicles were analogous to those of vesicles in the neurohypophysis. The absence of a chemical shift in the posterior pituitary has been considered a strong argument against a lipid cause for the bright signal, but phospholipids do not have any demonstrable chemical shift (Fig. 16). This paper opens the possibility of better understanding the source of bright signal in other cystic structures with abnormally bright signal and no chemical shift (see *AJNR* July/August, 1990).

Interventional Neuroradiology

Thirty-seven papers devoted to interventional neuroradiology were presented in 13 scientific sessions. Although the topics varied, most investigators continue to direct their efforts at improving the endovascular treatment of intracranial vascular abnormalities. In addition to the papers describing improvements in techniques and devices available for endo-

vascular procedures, other excellent papers described techniques of pre- and intraembolization functional testing and assessment of vascular reserve.

Of particular merit was "Endovascular Occlusion by Electrothrombosis of Experimental Small and Medium-Sized Saccular Aneurysms," by Guglielmi et al. (Rome and Los Angeles). This communication described the induction of intraaneurysmal thrombosis through the use of low-voltage electrical current (0.5 mA/2 V) passed through a small stainless steel guidewire fitted with a platinum tip. After adequate thrombosis is achieved, the platinum tip is detached from the stainless steel part of the guidewire by slightly increasing the voltage. These investigators described and illustrated this technique in a swine aneurysm model (Fig. 17). Three patients already have been treated successfully with this technique. Although this work is limited and preliminary, the results are encouraging. If this technique can be used to induce controlled thrombosis without distal embolization and to control coil positioning and detachment precisely, it will offer a major advantage over currently used methods.

The 1990 President's Lecture in honor of D. Gordon Potts was presented by Gazi Yasargil, a world leader in neurosurgery from Zurich, Switzerland. Dr. Yasargil recalled that the last ASNR meeting that he attended was in New York in 1964, at which time 80% of the audience was composed of neurosurgeons. He remarked that now a much larger ASNR audience included only one or two.

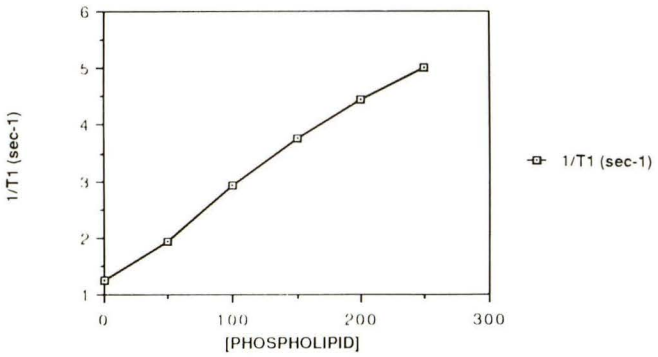

Fig. 16.—Graph shows T1 relaxivity as a function of phospholipid concentration (mg/ml). T1 relaxivity is linearly dependent on phospholipid concentration (r = 1.00) over entire range tested (0–250 mg/ml). No chemical shift of signal occurred.

Yasargil proposed that mastery of the arachnoidal system has been the key to the CNS for neurosurgeons, and he philosophically reviewed some of the developments of neurosurgery and neuroradiology, with some imagery borrowed from Greek philosophers. Highlighted historical figures included Roentgen, Dandy, Moniz, and Luessenhop as pivotal to the development of endovascular therapy of the CNS.

Yasargil reaffirmed the main therapeutic options for problem vascular lesions: (1) conservative management, (2) radiation therapy, (3) interventional neuroradiology therapy, (4) neurosurgical therapy, and (5) combinations of the first four. He expressed the opinion that, in most cases, intracranial aneurysms and arteriovenous malformations (AVMs) can be handled by microvascular surgery. This includes most AVMs, which now can be resected without blood transfusion. His examples of cases in which embolization was used included selections stressing various risks and limitations of this treatment for brain AVMs and aneurysms. At the same time, he predicted that, if interventional neuroradiology becomes well established, neurosurgeons again may wish to do angiography, which they gave up some decades ago.

He summarized transluminal angioplasty for vasospasm as a technique with serious dangers and made cautionary remarks about its use as a substitute for medications that are now commonly successful. Regarding the treatment of aneurysms, he disclaimed the concept that aneurysms have simple necks and stressed that proper neurosurgical treatment reconstructs the neck of the adjacent affected artery rather than merely clipping it. He suggested that balloons or coils more likely would provide insecure closure because of corners of untreated neck remnants.

Regarding cerebral AVMs, Yasargil said that angiography followed by surgery remains the best approach to understand the complete angioarchitecture of these lesions. He reiterated the approach of many neuroradiologists, that it is extremely important to visualize the venous as well as the arterial aspects of AVMs. He went on to say that he does not

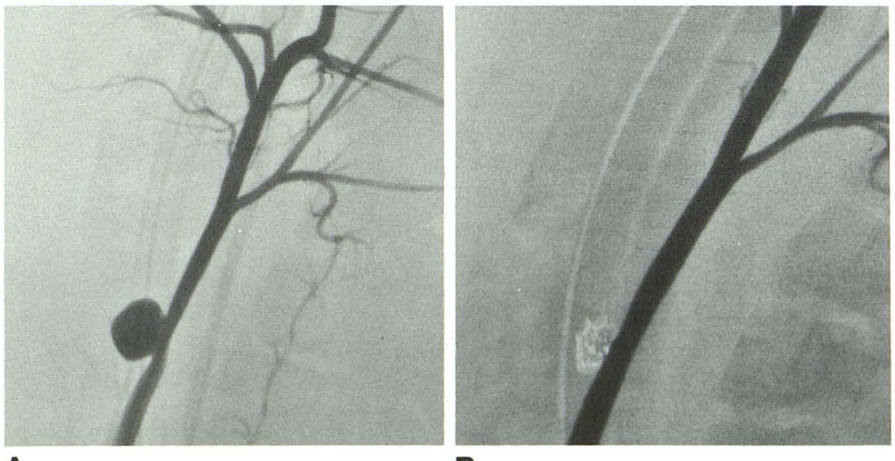

Fig. 17.—Intraaneurysmal thrombosis induced by using low-voltage electrical current.

***A*, Right common carotid arteriogram shows common carotid aneurysm created 15 days before treatment with low-voltage current.**

***B*, Right common carotid arteriogram shows area of aneurysm 3 months after embolization with five helical, platinum, detachable microcoils.**

understand why occlusions of veins are associated with brain AVMs and that the interactions between hemodynamics, neurologic function, electrical activity, and so forth are all rather complex.

He thinks that the entire brain is eloquent, with some areas that we do not understand, and he remarked that *lesions*, not the *brain*, should be attacked. A potpourri of examples of various types of cases undergoing interventional neuroradiology was shown, most of which stressed major risks of these procedures. He also stressed cooperation between interventional neuroradiologists and neurosurgeons in these treatments, including a critical review of results. One of his closing comments, taken from the Hippocratic Oath, "help or don't damage," was a summary of his message to the ASNR.

Stroke and Vascular Disease

The MR findings of acute stroke were reported by two groups. Bryan et al. (Baltimore) reviewed the findings in 44 patients with acute stroke and showed a high level of detection and sensitivity of ischemic infarction on spin-density and T2-weighted images. A fair proportion of these cases showed increased volume of affected brain on follow-up MR several days later. Yuh et al. (Iowa City) presented 23 patients who had MR imaging within 24 hr of acute ischemia. Spin-density and T2-weighted images showed no obvious signal change in some cases, especially those done within the first hours. Presumably the discrepancy between the conclusions of these two papers is related to the cases studied within 2 hr of the onset of stroke in the series of Yuh et al. These authors stressed the lack of flow void within affected arteries and enhancement (Fig. 18) of those affected arteries after IV administration of gadopentetate dimeglumine. They also found brain swelling on T1-weighted images and unusual parenchymal enhancement in some cases after administration of contrast material. They recommended that gadopentetate dimeglumine be used as part of the MR study of acute ischemic stroke, certainly a controversial conclusion.

Four presentations addressed MR evaluation of occlusive disease of carotid, vertebral, and affected intracranial arteries related to ischemic disease. Lane et al. (Philadelphia) correlated 49 MR imaging studies with angiography done within 60 days of the MR. Seventy-five percent of the carotid occlusions were identified as absence of the usual flow void and presence of increased intraluminal signal on routine spin-echo images. However, 47% of the high-grade stenoses were not identified on the standard MR studies. Schwaighofer et al. (San Diego) used spin-echo, T1-weighted, and gradient-echo images in 16 studies of patients with vertebrobasilar disease, including aneurysms, dolichoectasia, and occlusive disease, and concluded that MR was an effective evaluation technique. Kelly and Halbach (Travis Air Force Base, CA) emphasized three criteria for the evaluation of embolic stroke: (1) direct signal characteristics of the thrombus within affected vessels, (2) flow changes or lack of flow void within affected circulations, and (3) parenchymal changes. They noted that differences between "white thrombus" and "red thrombus" potentially could be differentiated on T2-weighted MR images. They speculated that white vs red thrombus identified on MR images may correlate with different causes and potentially different treatments, obviously work to be done in the future. Reversible parenchymal changes in affected ischemic areas also were discussed.

Boyko (Durham) reported on 14 patients who received IV gadopentetate dimeglumine and had loss of the usual arterial flow void on T1- and T2-weighted images. He stressed that contrast enhancement of intraluminal clot could not be differentiated from contrast enhancement of slowed flow.

AVMs and Vascular Diseases

Marks et al. (Stanford) presented results of heavy-particle Bragg peak radiosurgery for intracranial AVMs, reporting on more than 150 patients, of whom 101 had follow-up longer than 2 years. Eighty percent of these had high-flow AVMs. Of those malformations less than 4 cm in size, angiograms showed complete obliteration in 94% at 2 years and in 100% at 3 years. Of all the patients with follow-up angiograms, 62% had complete obliteration, 28% had partial obliteration, and 10% showed no change. Longer follow-up studies are needed

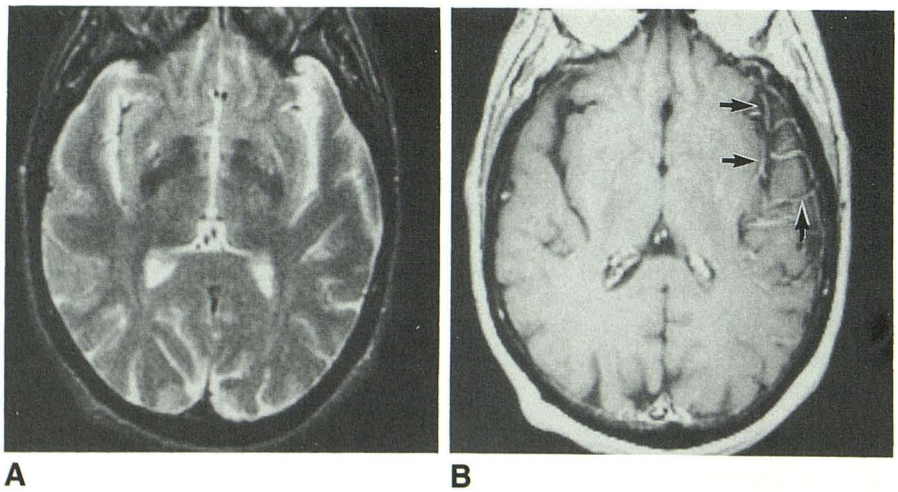

Fig. 18.—*A*, T2-weighted axial MR image obtained soon after a stroke involving left middle cerebral artery (MCA) shows absence of flow void in MCA branches in left sylvian fissure. Parenchymal abnormalities are not obvious.

***B*, T1-weighted MR image obtained after administration of contrast material shows MCA branches in sylvian fissure and over left operculum to be unusually enhanced (*arrows*). This was interpreted as slow flow in affected vessels due either to small branch outflow occlusions or collateral to a more proximal occlusion.**

for true comparisons of the clinical outcome, especially the rate of rehemorrhaging in comparison with the natural history. The last 40% of patients received lower doses than the earlier patients did, and no complications were reported.

Berenstein et al. (New York) reported on eight sets of monozygotic twins in which one twin of each set had some vascular anomaly and the other did not. Lesions included facial angiomas, cystic hygromas, cerebral AVMs, and cerebral arteriovenous fistulas. On the basis of these cases, it was suggested that these lesions are unlikely to be hereditary, although they may be congenital.

Dillon et al. (San Francisco) evaluated venous outflow in 39 patients with brain AVMs who were having MR imaging. The authors correlated the various patterns of varices, tortuous veins, and obvious narrowings with hemorrhage. In the category of severe venous outflow restriction with obvious collaterals, which was noted in nine of the cases, eight had presented with hemorrhage. However, when all signs of venous restriction, rather than just severe ones, were examined, the correlation with hemorrhage was poor. The main conclusion was that MR imaging was as accurate as angiography in identifying venous restriction in the outflow of brain AVMs.

Willinsky et al. (Toronto) reported on four patients who had dural arteriovenous malformations in the cervical and foramen magnum regions; the diagnosis was not made until surgery in three of the four. The clinical manifestations of the four cases included myelopathy, subarachnoid hemorrhage followed by myelopathy, numbness and weakness on one side, and tinnitus.

Contrast Agents

The safety and usefulness of a nonionic form of gadolinium, Gd-DTPA bis-methylamide (Gd-DTPA-BMA), in MR imaging of the brain and spine was discussed by two groups, Sze et al. (New Haven) and Bryan et al. (Baltimore). None of the 49 patients in the New Haven group suffered any significant side effects. Twenty-nine of 40 adults in the Baltimore series did not report adverse reactions within the 24-hr follow-up; the remaining patients complained of headache, rash, or nasal congestion. Laboratory blood tests and urinalysis showed no significant changes after administration of the contrast material. Both groups found satisfactory enhancement of normal anatomy and pathologic changes with Gd-DTPA-BMA and thought that this new nonionic MR contrast agent could be used safely as an alternative to gadopentetate dimeglumine.

Jinkins et al. (San Antonio) reported that iodinated radiographic contrast agents had an influence on MR images of the CNS. MR signal intensity was affected by contrast media given intrathecally and intravenously when subjects were scanned within 1 hr after injection. The T1 and/or T2 shortening that occurred led to an alteration in the observer's ability to detect certain pathologic changes.

Spine

Post et al. (Miami) reported on the cine-MR of spinal CSF flow in 26 healthy adults. Average peak caudal CSF flow rates ventrally were 25.7 mm/sec at C2, 50.5 mm/sec at C3, 50.5 mm/sec at C4, 28.0 mm/sec at L1, and 17.2 mm/sec at L4.

Schellinger et al. (Washington) introduced a flow-sensitive pulse sequence for detecting CSF pathway blockage in the spinal canal. A modified, steady-state, gradient-echo, nongated, 3D sequence was used, and images were acquired in only 2 min. The technique was used in 50 patients with spinal canal stenosis due to a variety of causes. Total occlusion of the canal could be diagnosed on the basis of the absence of flow signals approximately 3 cm rostral and distal to the blockage (Fig. 19). In subtotal obstruction, persistence of flow could be verified by maintenance of the flow signals. This new slow-flow MR sequence was thought to obviate myelography. Levy et al. (Baltimore and Bethesda) assessed longitudinal pulsatile motion of the spinal cord in 75 patients. They used spinal echo-phase (velocity) imaging, often combined with MR tagging techniques and gradient-echo phase-contrast cine-MR, to study the normal caudal motion of the spinal cord and to contrast the findings with those of cases of cord tethering and cord compression. They saw a marked decrease in cord motion in symptomatic patients who had tethered cords, in symptomatic postoperative patients who had retethered cords, and in patients who had cord compression (Fig. 20).

Sherman et al. (New York) presented an important paper on the ability to determine clinical significance and prognostic importance of the heterogeneous appearance of vertebral bone marrow occasionally seen on short TR MR images in patients without a known malignancy or marrow disorder. Although irregular areas of variable marrow signal intensity on short TR images appeared to be an age-related phenomenon, they were indistinguishable from those seen in metastatic disease. However, diffuse or discrete areas of hypointensity, especially areas less intense than those of the intervertebral disk, were thought more likely to represent neoplastic marrow replacement in this series of 45 patients.

Sze and Gero (New Haven) presented the MR findings in intradural inflammatory disease of the spine in 22 patients. They found several features that were more likely to occur in nongranulomatous infectious myelitis than in tumor. These features were (1) diffuse high intensity of the cord on long TR images out of proportion to the amount of cord swelling and either (2) diffuse enhancement of the cord with injection of contrast medium or linear enhancement along the margins of the cord or (3) no contrast enhancement. In cases of granulomatous myelitis, such as in tuberculosis, distinction from neoplasm was more difficult.

Excerpta Extraordinaire

Two novel therapeutic approaches to life-threatening situations were reported as part of the interventional section of the excerpta extraordinaire. Lane and Marks (Stanford) described a therapeutic approach to an actively leaking cerebral aneurysm that was noted to be extravasating during angiography. On an emergency basis, they treated the aneurysm by balloon occlusion and subsequently effected a cure by using platinum microcoil embolization. Deveikis et al. (Washington)

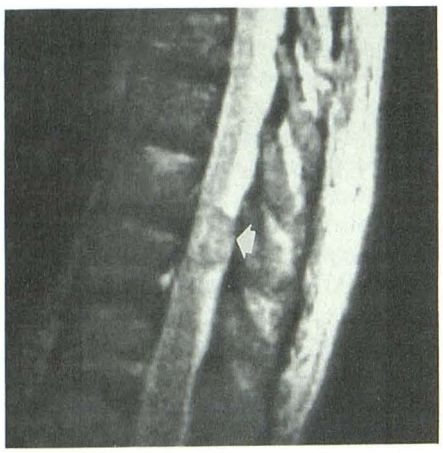

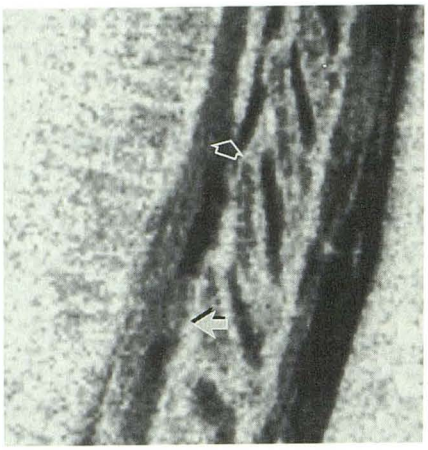

A B

Fig. 19.—Intradural extramedullary mass causing total or near-total obstruction of low thoracic canal.

A, Spin-echo T2-weighted MR image, 2000/90, shows lesion (*arrow*) with bright CSF as expected.

B, Slow-flow MR image shows lesion (*solid arrow*). About two vertebrae above lesion, CSF turns from white to black (*open arrow*), denoting ultraslow flow or CSF stasis. CSF below lesion is black also.

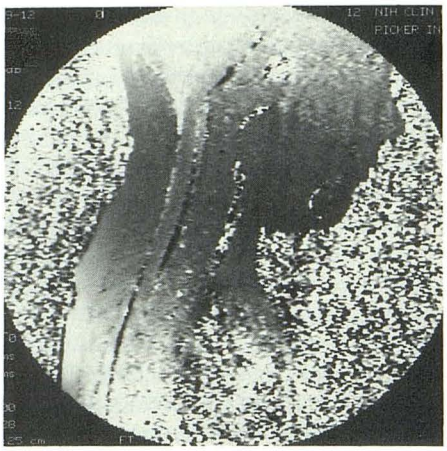

Fig. 20.—Phase (velocity) image of cervical spine in a symptomatic girl with myelodysplasia and tethered cord. In early systole, CSF flow reversal can be observed in spinal canal (black or cephalad anteriorly, white or caudad posteriorly). However, spinal cord motion was absent (gray signal). After surgical untethering, spinal cord motion became normal.

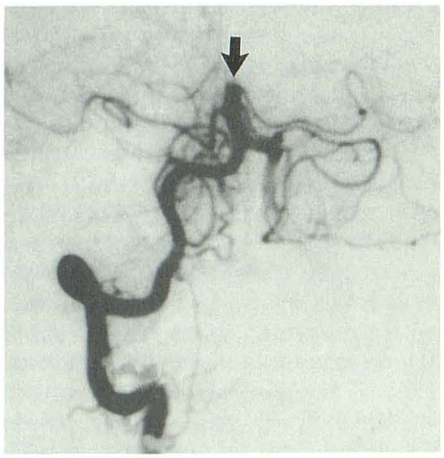

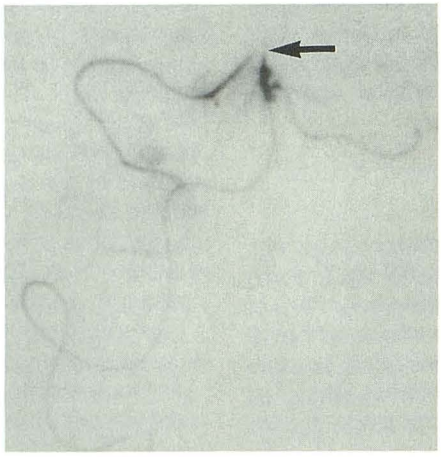

A B C

Fig. 21.—Treatment of an actively leaking cerebral aneurysm.

A, Right vertebral arteriogram shows occlusion of basilar artery by thrombus (*arrow*).

B, Digital subtraction arteriogram through a microcatheter shows that tip of catheter is at level of thrombus (*arrow*). Urokinase was injected here.

C, Anteroposterior view during control arteriogram after local intraarterial thrombolysis shows basilar artery is now patent (*arrow*).

delivered local intraarterial, intrathrombus thrombolytic therapy (urokinase) to a basilar artery thrombosis in an acutely quadriplegic and comatose 24-year-old woman who had a left vertebral artery dissection and an occluded basilar artery. This treatment resulted in almost complete disappearance of neurologic symptoms within 24 hr (Fig. 21).

Russell (Chicago) found that an unusual venous anomaly associated with severe dural venous sinus stenosis or hypoplasia was the cause of tinnitus in two patients (Fig. 22). Rapid flow in the stenotic vein caused the local bruit. In one case, direct catheterization resulted in moderate distension of the stenotic segment.

Epidural spinal pneumatosis, a benign entity in trauma victims, was presented by Willing (Louisville). Three patients with traumatic pneumomediastinum had dissection of air, seen incidentally on spinal CT, into the neural foramen and epidural space.

Weingarten et al. (New York) described an unusual case of tension pneumocephalus due to a ruptured viscus. The pneumocephalus was caused by the forced retrograde dissection of air along, but not within, the shunt tube in a patient who had been operated on for a medulloblastoma and in whom increased intraabdominal pressure developed because of perforation of a congenital colonic diverticulum (Fig. 23).

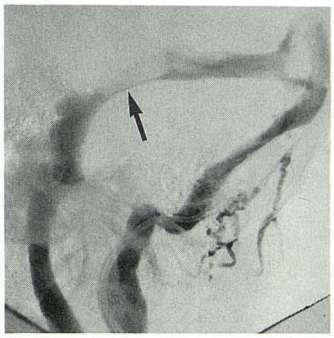

Fig. 22.—Oblique lateral view during venous phase of carotid arteriogram shows focal stenosis (*arrow*) of dural venous sinus, which caused tinnitus.

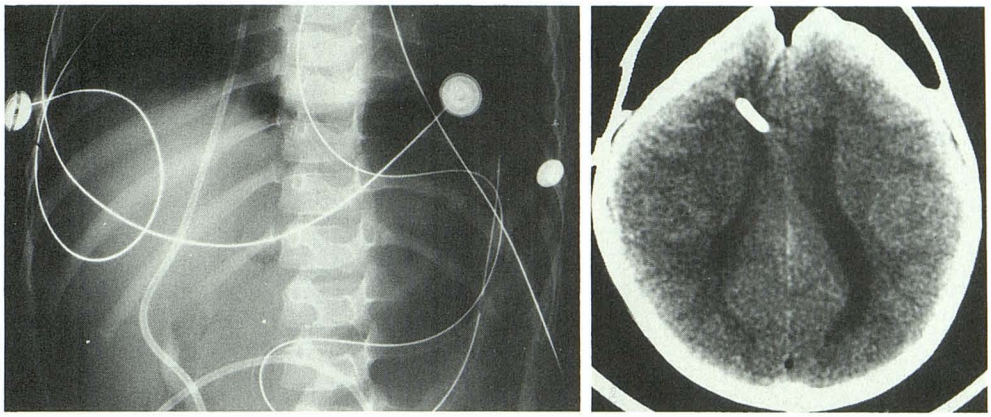

A B

Fig. 23.—*A*, Radiograph of supine patient shows free air in abdomen due to a ruptured viscus and peritoneal portion of shunt tube.
B, CT scan shows tension pneumocephalus.

Feaster et al. (Washington) described the CT and MR findings in wind instrument players who had vague clinical signs and symptoms of pharyngeal distension and progressive enlargement of the neck. Performance of modified Valsalva maneuver produced massive symmetrical air distension of the piriform sinuses and pharynx.

A rare, vascular, embryologic anomaly, fenestration of the internal carotid artery, in a 61-year-old woman with tinnitus and a mass in the hypotympanum was reported by Koenigsberg et al. (New Hyde Park, NY). The tinnitus was thought to be due to associated erosion of the cochlea (seen on CT), possibly in conjunction with deformity of the stapes due to a persistent stapedial artery.

Two rare cases of central neurocytoma, presenting with intraventricular hemorrhage, were reported by Rippe et al. (Orlando) and by Smoker and Reichman (Salt Lake City) (Fig. 24). These well-defined, supratentorial, intraventricular masses, which often are calcified, and which show contrast enhancement on both CT and MR, have a more favorable prognosis than do parenchymal neuroblastomas.

Hald et al. (Oslo) suggested that patients with bilateral arachnoid cysts be investigated for an enzyme deficiency, namely lack of glutaryl-CoA dehydrogense. In four cases of their own and in four previously reported cases, bilateral arachnoid cysts were detected on imaging studies in patients suffering from glutaric aciduria type 1, an uncommon inborn error of metabolism.

An unusual case of an intracranial intradural chordoma simulating a brainstem tuberculoma was reported by Hayne et al. (Seattle). MR showed a normal clivus and an adjacent, heterogeneously enhancing, extraaxial mass (Fig. 25).

Haimes and Krol (New York) described an important case of an exclusively extradural, dumbbell-shaped thoracic hemangioma that had no bone involvement and that mimicked tumors more commonly producing dumbbell-shaped spinal lesions. However, clues to the diagnosis were the extensive cephalocaudal epidural involvement and absence of an intradural component.

A fascinating case of spontaneous expulsive choroidal hemorrhage, a rare ophthalmologic emergency, was presented by Knopp and Chynn (New York). They pointed out the characteristic CT findings in this entity, namely soft-tissue protruding from the intact globe and scleral coat, the hemorrhagic nature of the process, and enhancement of the choroidal vessels.

Finally, Kuhn et al. (Springfield, IL) reported finding calcification in the abducens nuclei bilaterally on CT and MR, suggesting the diagnosis of Möbius syndrome, group III. This is a congenital neuromuscular disorder characterized by facial weakness and inability to abduct the eyes.

Epilepsy, Positron Emission Tomography, and Cerebral Blood Flow

A significant paper indicating the low level of efficacy in the use of gadopentetate dimeglumine in 150 prospectively studied seizure patients undergoing MR imaging, was presented by Elster et al. (Winston-Salem). Enhancement occurred in 22% and was helpful in only 13%. In only one case did a postcontrast study show significant abnormalities in an otherwise normal noncontrast study. Rauch et al. (Los Angeles) described the use of an MR-compatible stereotactic frame and electrodes. The stereotactic coordinates, determined by MR, gave 3-mm spatial accuracy in electrode placement. Lo et al. (Stanford) described an animal model in which MR imaging and positron emission tomography (PET) are used to show early and late delayed effects of radiation therapy. Rubidium-PET showed areas of activity corresponding to gadopentetate dimeglumine enhancement on MR. A paper describing the use of dysprosium-DTPA-BMA as an intravascular perfusion agent in MR imaging was presented by Frank et al. (Bethesda). This purely intravascular agent produces a change in signal intensity when it passes through the capillary beds in areas that have increased function because of visual stimulation. These findings correlated with PET-measured cerebral blood flow. Edelman et al. (Boston) used gadopen-

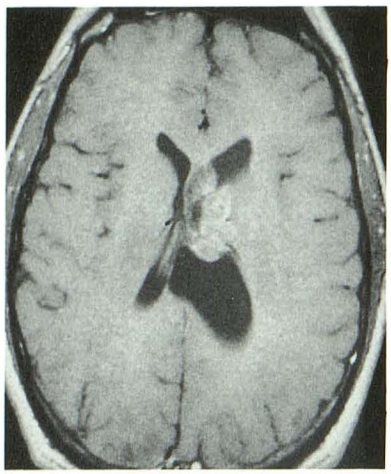

Fig. 24.—T1-weighted MR image obtained after administration of gadopentetate dimeglumine shows a mildly enhancing mass in left lateral ventricle that appears to arise from septum pellucidum. Diagnosis was central neurocytoma.

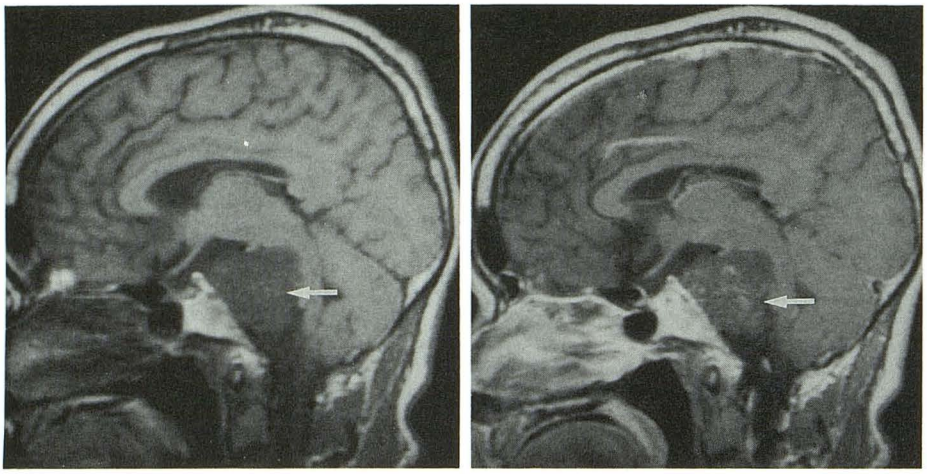

A B

Fig. 25.—Intradural chordoma.
A, Precontrast T1-weighted MR image, 600/30, shows an extraaxial heterogeneous mass (*arrow*) in prepontine cistern without destruction of clivus.
B, Postcontrast T1-weighted MR image, 600/30, shows patchy enhancement within mass (*arrow*).

tetate dimeglumine as a purely intravascular perfusion agent to detect areas of abnormal perfusion. This technique does not measure actual or true cerebral blood flow. Instead, one slice is selected, an area of interest is determined, and the relative perfusion through the area is compared with normal perfusion in other areas. The technique is not yet quantitative and is similar to techniques developed a decade ago to evaluate "transit time" by using the intravascular passage of a contrast agent during CT scanning.

Patronas et al. (Bethesda) evaluated the use of echo-planar sequences to evaluate perfusion through tumors in patients injected with gadopentetate dimeglumine. Echo-planar sequences are extrafast; each image requires only 100 msec to acquire. Although the passage of the contrast agent through capillaries was similar to that seen in the work of Edelman et al., the rapidity of the echo-planar technique allowed a better assessment of dynamic changes in the tumor beds. A major drawback of the echo-planar technique is the noise present in the images. Dean et al. (Lexington, KY) used a different sequence (turbo fast low-angle shot) during the rapid infusion of gadopentetate dimeglumine. Like the techniques in the earlier papers, this one does not determine true cerebral blood flow, as the material stays within the blood vessels. In this case, measurement was made of the blood pool within a region of interest.

Pistoia et al. (Pittsburgh) reported on the xenon-CT technique of determining cerebral blood flow in patients with severely low global blood flow compatible with the clinical determination of brain death. These low flows, over a prolonged period were indicative of diffuse ischemia or infarction. Global hyperemia was seen as a precursor of subsequent diffuse loss of autoregulation and indicated a grave prognosis. Stringer et al. (Richmond) compared portable xenon-133 evaluation of cerebral blood flow with the xenon-CT technique. They showed good correlation between the two techniques, so that the portable radioisotopic technique can be used at the bedside to follow the status of blood flow after more general data are obtained by using the xenon-CT technique.

Yonas et al. (Pittsburgh) reported on the manipulation of blood pressure during the xenon-CT measurement of cerebral blood flow to determine whether vasospasm is the cause of symptoms or whether hypertensive therapy will be effective. In two of seven patients, cerebral blood flow was raised above ischemic levels with an increase in blood pressure; in five other patients, there was no effect. Because hypertensive therapy may be dangerous, this is a good technique for determining its possible effectiveness.

Finally, Tarr et al. (Pittsburgh) described using the xenon-CT determination of cerebral blood flow to evaluate hemodynamic changes that occur after therapeutic embolization of AVMs. After embolization produced a decreased vascular bed, Diamox (acetazolamide), which normally produces increased cerebral blood flow, caused diminished augmentation of cerebral blood flow in areas in and around the AVM, indicating maximal vasodilatation in those areas. Three patients also had areas of hyperperfusion and decreased response to Diamox, which might reflect hemodynamic changes resulting in perfusion abnormalities in adjacent normal areas.